Zinc abundances of stars in the Milky Way

Max Haase

Lund Observatory
Lund University

2015-EXA96

Degree project of 15 higher education credits
May 2015

Supervisor: Thomas Bensby

Lund Observatory
Box 43
SE-221 00 Lund
Sweden

Abstract

In this work we study the spectra of 423 stars in the Milky Way disk in order to determine their zinc abundances. The methodology to determine elemental abundances consists of synthesising sets of spectra with varying zinc abundances and comparing them with the observed spectra to find the best fit. The aim of the project was to compare the spectra synthesis method used here to Bensby et al. (2014) where zinc abundances were determined for the same sample of stars using equivalent width measurements. The resulting abundances show a near zero [Zn/Fe] ratio with a slightly higher ratio in the $-1.3 < [\mathrm{Fe/H}] < -0.2$ interval. The spread in [Zn/Fe] ratios was not reduced compared to Bensby et al. (2014) and no improvement was observed from the spectra synthesis methodology. This shows that the relatively large scatter in [Zn/Fe] could be intrinsic and not due to the analysis methods. Furthermore, the results support the idea of core collapse supernova being the main contributor to interstellar zinc while type Ia supernova account for a minor contribution.

Populärvetenskaplig sammanfattning på svenska

Modeller som beskriver ämnesyntesen i stjärnor och supernovor har haft begränsad framgång med att förklara de observerade halterna i stjärnor. Dessa modeller är inkonsekventa för olika grundämnen och det saknas en komplett bild över den ämnesberikningen som sker i vårt universum.

Syntes av ämnen i stjärnor beror på många faktorer som ursprunglig kemiska sammansättning hos stjärnan, tillgänglig energi, stjärnans massa, etc. som tillsammans leder till olika kärnprocesser och slutgiltigt öde hos stjärnan. Vissa stjärnor berikar med mycket zink relativt järn medans andra berikar med lite zink relativt järn. Berikningshistorien som leder upp till bildningen av en viss stjärna bestämmer alltså zink/järn-kvoten. En viss population av stjärnor förväntas därför ha en viss zink/järn-kvot enligt ämnessyntesteorier. I detta projekt testar vi hur bra detta stämmer.

Spektroskopi är en av de främsta verktygen vi har för att studera himlakroppar. I ett spektrum kan man finna information om en stor mängd egenskaper hos källan. Till exempel påverkas spektrat av fysiska egenskaper som temperatur, relativ hastighet, gravitation, etc. men det är även ett sorts fingeravtryck för den kemiska sammansättningen hos objektet.

I det här arbetet bestämde vi zinkhalter för en mängd stjärnor i Vintergatans disk för att undersöka hur zinkhalten förhåller sig till järnhalten i stjärnor. Med denna information kan vi testa de teoretiska modelerna för zinksyntes i olika typer av stjärnor och på så sätt få en bättre uppfattning om zinks ursprung. En väldefinierad trend för zink i förhållande till järn kan även vara användbart för att uppskatta järnhalter hos mycket avlägsna objekt. Detta är på grund av svårigheten att direkt bestämma dessa järnhalter eftersom de spektrallinjerna som normalt sätt används för detta absorberas av det intergalaktiska mediet. Spektrallinjerna som används för att bestämma zinkhalter lider inte lika mycket av detta fenomen vilket gör det mer praktiskt att använda zink för att bestämma järnhalten i dessa objekt.

För att bestämma zinkhalterna syntetiserades spektra med varierande zinkhalt som sedan jämfördes med de observerade spektra. Det syntetiska spektrum som passar bäst bestämmer då zinkhalten hos stjärnan. Detta gjordes för 423 olika stjärnor i Vintergatans tjocka och tunna disk.

Resultaten visar ingen märkbar reducering i spridningen av zinkhalter jämfört med halterna från Bensby et al. (2014). Detta tyder på att metoden inte är bättre än den som användes av Bensby et al. (2014) på att bestämma zinkhalter. Det är inte säkert om denna spridningen i zink halter beror på problem med metoderna som har använts eller om det är på grund av en verklig spridning i halterna.

Resultaten stöder hypotesen att det framförallt är typ II supernovor, dvs kollaps av massiva stjärnor som står för zinkberikningen i universum. Typ Ia supernovor, orsakade av lå g massiva stjärnor, producerar förmodligen försummbara mängder av zink jämfört med järn. Detta leder till en minskning av zink i förhållande till järn ju mer metallrik ett objekt är eftersom denna typ av supernova sker mer i metallrika stjärnor.

Om det är lämpligt att använda zinc som ett surrogatämne till järn vid bestämningen av järnhalter beror på den önskade precisionen. Standardavvikelsen av Zn/Fe kvoten är

0.12 dex vilket fungerar som ett mått på det förväntade felet vid bestämning av järnhalter med denna metoden.

Contents

Chapter 1

Background

1.1 Introduction

Accurate stellar elemental abundances are important in order to have reliable constraints for stellar nucleosynthesis models. Zinc lies just beyond the iron peak elements and has no stable isotopes produced by α processes. Zinc is a particularly important element for supernova physics (e.g. Nomoto et al. 2013). Zinc is also of particular interest because it is a potential surrogate element for iron when determining the metallicity of distant objects, such as damped Lyman-alpha systems. The spectral lines typically used to determine iron abundances are susceptible to extinction in the intergalactic medium. Zinc abundances seem to trace iron abundances for a wide range of metallicities. Zinc lines are also observable in distant objects whose light has suffered a large amount of extinction. Using zinc as a proxy for iron is particularly useful for studying metal poor damped Lyman alpha systems (Kobayashi et al. 2006) where traditional methods of determining iron abundances seem futile.

The reason for zinc being a potential proxy for iron is that they follow a similar abundance trend for a wide range of metallicities. This similarity could be explained by zinc and iron production being proportional to each other for the main enrichment processes. However, the large spread in [Zn/Fe] observed in Galactic disk stars suggests that the relative production of zinc and iron could vary for different sources. One of the purposes of this project is therefore to investigate if this proportionality is present for the various zinc and iron sources. Even without a perfect proportionality, a corresponding iron abundance for a given zinc abundance could be obtained if the [Zn/Fe] ratio follows a predictable trend. These results will hopefully also shed some light on which zinc sources are the most significant and which theoretical models best explains this.

1.2 Theoretical sources of zinc

Theoretical models that calculate the the expected elemental yields from stars of different types and fates have had an unsatisfactory precision and are often inconsistent. Although

the probable sources of zinc are known, the precise magnitude of their contribution to the overall zinc abundance is debatable.

Most of the zinc is believed to come from explosive nucleosynthesis in supernovae (SNe) and hypernovae (HNe), which in this work is any supernova with a released energy exceeding 10 foe[1].

Depending on the mass and metallicity of the progenitor, the released energy and the nature of the supernova, the amount of zinc that is produced and cast out into the interstellar medium varies greatly. More importantly for this work, the ratio of zinc to iron may also vary by several orders of magnitude. When many different enrichment sources can occur the final product is likely to have a [Zn/Fe] ratio that is averaged over the possible sources, weighed by the magnitude of their individual contribution and by their prevalence.

Attempts to model zinc yields from SNe have resulted in [Zn/Fe] ratios that decrease with the mass of the progenitor for low metallicity stars ($Z \leq 0.001$)[2] (e.g. Kobayashi et al. 2006). According to this model, progenitors with $Z = 0, M \geq 25 M\odot$ result in SNe with negligible zinc yields relative to the iron yield (compared to the solar ratio). In the model proposed in Tominaga et al. (2007) the Zn/Fe ratio of the yield of low mass, Z=0 SNII should be slightly lower than zero. For high metallicity progenitors ($Z \geq 0.004$) the [Zn/Fe] ratio is instead expected to increase with the mass of the progenitor (e.g Kobayashi et al. 2006). Massive high metallicity stars resulting in SNe are potentially one of the main sources of high [Zn/Fe] ratio enrichment, rivalling HNe.

The more energetic HNe generally produce a greater amount of zinc compared to iron. They are also less sensitive to the effects of metallicity and mass of the progenitor with HNe of all metallicities producing yields with high [Zn/Fe]. Kobayashi et al. (2006) calculated the [Zn/Fe] yield of 10-30 foe, 20-40 $M_\odot$ HNe to be between 0 and 1 for metallicities ranging from zero to solar value (Z = 0.02). Tominaga et al. (2007) also consistently got [Zn/Fe] ratios in the 0-0.5 range from their extremely metal poor HNe models. HN are two to three orders of magnitude less common than SNII (Podsiadlowski et al. 2004). Although HN result in large ejected masses, this rarity still suggests that HN are much less significant than SNII when it comes to elemental enrichment. However, a single HN could account for a large fraction of the enrichment of a low metallicitiy star and could explain some of the large [Zn/Fe] ratios of low metallicity stars.

Although SNIa may result in large Zn yield, the [Zn/Fe] fraction is probably very small due to SNIa also producing large amounts of Fe (e.g. Nomoto et al. (1997)). In the SNIa models described in Nomoto et al. (1997), the expected [Zn/Fe] ratio of the yield is approximately two to five times smaller in absolute terms compared to the yield of SNII.

SNIa are believed to have a negligible contribution to Milky Way stars with [Fe/H] < -1.1 due to a delayed enrichment from SNIa (Kobayashi & Nomoto 2009). The low rate of SNIa in low metallicity populations are not observationally confirmed and there is evidence of the contrary (e.g. Prieto et al. 2008). Even for higher metallicity stars, SNIa account

[1] 1 foe = 10^{51} erg = 10^{44} J; stands for (ten to the power of) fifty one ergs.

[2] the Z metallicity is the fraction of matter heavier than helium in a star. As a reference, the Sun has Z = 0.02.

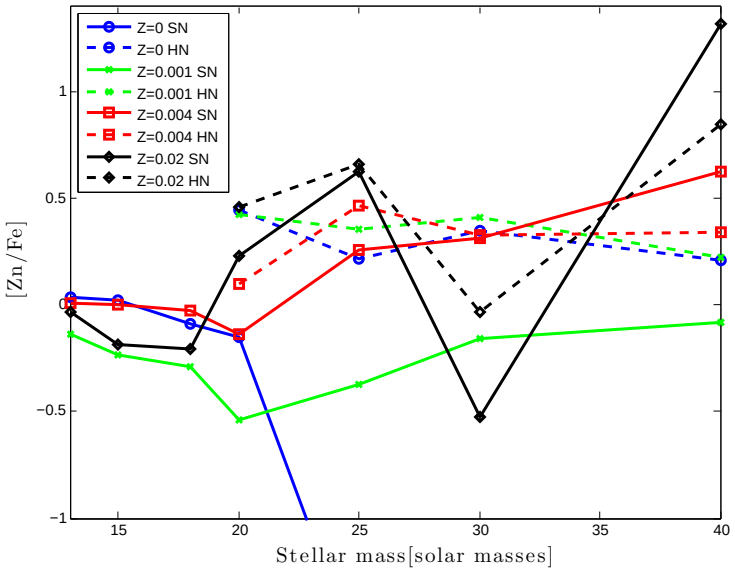

Figure 1.1: Zn yields obtained by Kobayashi et al. (2006) for stars of different masses and metallicities. Z=0, Z=0.001, Z=0.004 and Z=0.02 are shown with blue circles, green crosses, red squares and black diamonds respectively. Solid lines show 1 foe SNe and dashed lines show HNe(10 foe for 20 and 25 $M\odot$ 20 foe for 30 $M\odot$ and 30 foe for 40 $M\odot$)

for a minority of the total amount of SNe (Kobayashi & Nomoto 2009). However, the high Fe yield of SNIa could mean that even with a low occurrence rate (N_{SNIa}/N_{SNII}=0.15 (Tsujimoto et al. 1995)), approximately half of the Fe of high metallically stars is expected to come from SNIa (Nomoto et al. 1997).

Since the zinc production relative to iron production in SNII is higher for progenitors with higher metallicity, the [Zn/Fe] ratio is at first expected to go up with increasing metallicity. However, once it reaches the threshold for SNIa to occur at [Fe/H] = −1, the [Zn/Fe] ratio will start declining with increasing metallicity (e.g. Kobayashi & Nomoto 2009). This should result in a increase in the [Zn/Fe] ratio for stars with metallicities in the range $-1.5 \leq$ [Fe/H] ≤ -1.

1.3 Observations of zinc in the Milky Way

Bensby et al. (2014) determined zinc abundances for 714 stars in the Milky Way thin and thick disks (blue asterixes in fig. 1.2). The abundance for a lower metallicity sample of 87 thick disk and halo stars was determined by Ishigaki et al. (2013) (red crosses in fig. 1.2). These studies used a equivalent width based methodology to determine the zinc abundances. The resulting [Zn/Fe] ratios have a relatively large spread that is similar for both studies and decreases slightly at lower metallicities. The [Zn/Fe] ratios from Bensby et al. (2014) have a spread of more than double that of [Cr/Fe] and [Ni/Fe] which are the other

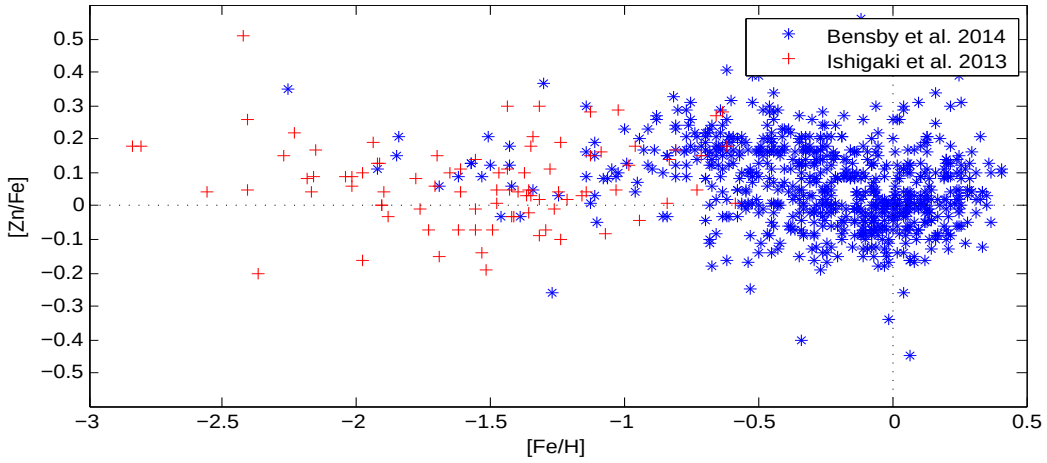

Figure 1.2: Zinc abundance results from Bensby et al. (2014) (blue asterixes) and Ishigaki et al. (2013) (red plusses).

iron-peak elements that were determined by the same study using the same methodology. Whether this spread is intrinsic for the stars or if it is caused by the methodology is unclear but since these studies are based on equivalent width measurements there could be issues with blending spectral lines that are not accounted for when measuring the strength of the zinc lines. For solar metallicity stars this error should be mostly accounted for when normalising with respect to the Sun. However, it should also result in an error that increases as the metallicity of the star decreases because the contribution from the blending lines decreases with the metallicity of the star while the change in abundance from normalising with respect to the Sun remains the same.

The average [Zn/Fe] ratio is near zero or slightly above at all metallicities but with a small increase at around $-1.1 < \text{[Fe/H]} < -0.75$. Although it is a smaller increase and is at a higher metallicity than expected by the reasoning presented in sect. 1.2, the presence of this local increase in [Zn/Fe] supports the idea of more zinc relative to iron being produced by SNII at higher metallicities and a lower amount of zinc relative to iron being produced by the delayed SNIa. However, at very low metallicities there also appears to be a higher [Zn/Fe] ratio which is not consistent with the predicted low zinc yield from low metallicity SNII, although this could be due to the small sample of stars with $\text{[Fe/H]} < -2$. A large number of high energy HNe in low metallicity populations could also explain such an increase the [Zn/Fe] ratio.

1.4 Aim of this thesis work

The goal of this thesis work is to investigate the precision of the zinc abundance results obtained by Bensby et al. (2014) by using a different methodology. As stated in sect. 1.1, accurate zinc abundances are essential for determining whether or not zinc can be used as a proxy for iron. Accurate zinc abundances are also important to determine the success

of different stellar nucleosynthesis models, particularly for models concerning SNII and SNIa yields. The results from this work will also give insight into how the equivalent width measurements and the spectra synthesis methods compare when determining zinc abundances.

Chapter 2

Method

2.1 Software

The IDL software Spectroscopy Made Easy (SME; Valenti & Piskunov (1996); Valenti & Fischer (2005)) was used to synthesise the spectra. SME is a software package capable of producing synthetic spectra for a model atmosphere as well as fitting these spectra with high resolution observed spectra in order to determine stellar parameters. In this work we only use SME to obtain the synthetic spectra which we then fit to the observed spectra in the MIDAS[1] environment. For each synthetic spectra, the model atmosphere is parameterised with the effective temperature, surface gravity, microturbulence, [Fe/H] ratio and rotation velocity of the star that the observed spectra was taken from. SME can use VALD3 line data in order to synthesise the spectral lines present in a wavelength interval. A script written in the MIDAS command language was used to initiate SME with the appropriate parameters and then fit the observed spectra with the resulting synthetic spectra. The fitting process involved a wavelength shift to account for the doppler shift of the star. The next step was to adjust the continuum level of the observed spectra by addition of a first degree polynomial intended to align the parts of the synthetic and observed spectra that were relatively void of spectral lines. The MIDAS script then calculated the sum of the squares of the difference in normalised flux for each discrete wavelength in the spectra (denoted by ζ)[2] in order to determine which synthetic spectra best coincides with the observed spectra. The abundance of the synthetic spectra that resulted in the smallest ζ was used as a starting point for the synthesis of a new set of synthetic spectra with a smaller abundance step (0.06). The final abundance was the one used to synthesise the spectra with the smallest ζ in this refined analysis.

[1] ESO-MIDAS is the acronym for the European Southern Observatory Munich Image Data Analysis System which was developed by the European Southern Observatory

[2] $\zeta \propto \sum \chi^2$

2.2 Stellar sample

The sample contains F and G dwarf and subgiant stars in the thin and thick Galactic disks in the Solar neighbourhood. The sample of stars used are a subset of the stars in Bensby et al. (2014), who obtained the spectra with the MIKE spectrograph (Bernstein et al. 2003) on the 6.5m Magellan Clay telescope on Las Campanas in Chile. A spectral resolution of $R = 65000$ was used for 374 stars and $R = 42000$ for 49 stars in the sample. The spectra have a signal to noise ratio of $S/N = 150 - 300$. The metallicities, kinematic properties, effective temperature, surface gravity and microturbulence of the stars were taken from Bensby et al. (2014).

2.3 Synthesising the spectra

In order to determine the zinc abundances of the selected stars we produced sets of synthetic spectra with varying zinc abundances and compared these with the observed spectra to find the best fit. For each observed spectra a set of ten synthetic spectra was produced with a set temperature ($T_{\rm eff}$), micro-turbulence (ξ), surface gravity ($\log g$), [Fe/H] ratio and rotation velocity. The doppler shift and rotation velocity of the stars was estimated by analysing three spectral lines for iron at 6065Å, 6546Å and 6678Å. The doppler shift was obtained by shifting the observed spectra until the spectral lines of the observed and synthetic spectra coincide and the rotation velocity was obtained by fitting synthetic spectra to the observed spectra around these lines with varying rotation for the synthesised lines. The metallicity of the star was also used to estimate the strength of all spectral lines besides the zinc lines. The log gf values for all the synthesised lines were obtained from the VALD3 database (Piskunov et al. 1995; Kupka et al. 1999; Ryabchikova et al. 1997; Kupka et al. 2000) and are shown in Tables A.2, A.3, and A.4. SME was used to synthesise the spectra and a MIDAS script was used to fit the observed and synthesised spectra. This was done by shifting the wavelength of the observed spectra to account for the doppler shift and adjusting the continuum of the observed spectra to coincide with the synthesised spectra. For the 6362Å spectral line it was sufficient to use the wavelength shift obtained by studying the iron lines. However, for the 4722Å and 4811Å lines it was necessary to apply a small adjustment to this shift in order for the zinc spectral lines to coincide properly. This offset could be because of an imperfect agreement between the red CCD that was studied to determine the wavelength shift, and the blue CCD where the 4722Å and 4811Å spectral lines are situated. The abundance of the synthetic spectra that resulted in the smallest χ^2 was used as a starting point for the synthesis of a new set of ten synthetic spectra with a smaller abundance step (0.06). The synthetic spectra that resulted in the smallest χ^2 in this refined analysis determined the zinc abundance. The lines used for the comparison between the synthetic and observed spectra were situated at 4722Å, 4810Å and 6362Å. The final absolute abundances were obtained by taking the mean of the abundances from the individual lines. Some of the spectra could not be analysed accurately either due to the Zn line being too weak (particularly for the relatively weak 6362Å line) or because

of numerical difficulties when comparing the observed spectra with the synthetic spectra. The excluded spectra are listed in Table B.1 along with the reason for their exclusion. Figure 2.1 illustrates how the synthetic and observed spectra were aligned and compared in order to determine which zinc abundance resulted in the best fit.

The zinc abundances along with several other abundances have already been determined for this sample (Bensby et al. 2014). However, this was done with another methodology. The spectral synthesis method used in this project will hopefully yield more precise results where any underlying trends are easier to distinguish. One of the weaknesses of the equivalent width based measurements is that they do not take into account superposed spectral lines of other elements. In order to test if this is the case for our spectral lines we synthesised spectra for the three spectral lines without the zinc line with the stellar parameters of the relatively high metallicity ([Fe/H] = −0.1) star HIP56557 (see fig. 2.2). There is clearly a problem with contamination for the 4722Å and 4811Å lines but the 6362Å looks like it should be fine with equivalent width measurements in all except the highest metallicity stars. This means that equivalent width based measurements should have a tendency to overestimate the zinc abundance when measuring the 4722Å and 4811Å spectral lines. Solar analysis should partly cancel this effect for stars with a similar metallicity as the Sun since the solar abundance will be overestimated by the same amount. From the line data obtained from VALD3, the 4722Å line is blended with a combination of weak lines from Fe, Cr, Sr, Ce and C_2. The 4811Å line is blended with a Cr line. These abundances are therefore of particular importance to further improve the results, although in this work all abundances except for zinc was simply scaled from the [Fe/H] ratio.

2.4 Solar analysis

Once the absolute abundances had been determined, we used the same method to determine the zinc abundance for a set of solar spectra. Here we use the solar spectra obtained form observations of sunlight reflected on Vesta and Ceres. The average logarithmic solar abundance was then subtracted from our logarithmic stellar abundances to give the abundance relative to the Sun. This is done so that the values can be compared to other abundance studies. This should also help to minimise any systematic errors that may arise from our method since the same systematic error should be present in the abundance obtained for the Sun, at least for stars with close to solar metallicity. The final zinc abundance was obtained by taking the average normalised abundance for the three zinc lines that we analysed.

2.5 Uncertainties

The stellar sample has uncertainties in effective temperature, surface gravity, [Fe/H] and microturbulence. To see how these uncertainties could affect the final abundance result we took six spectra that were spread out in the parameter space and determined the

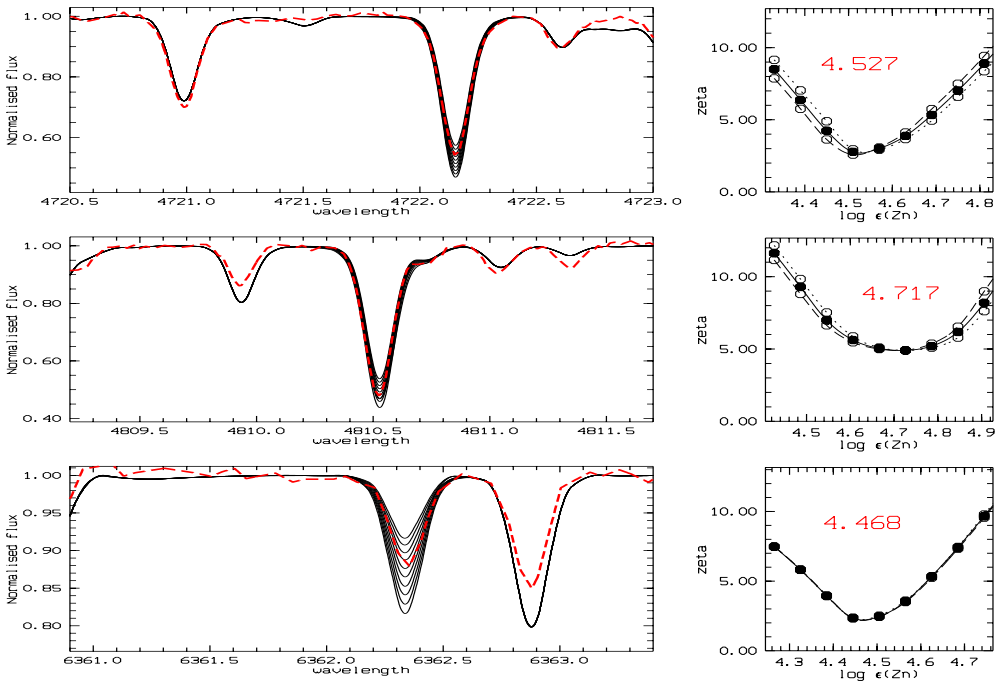

Figure 2.1: Visual representation of the observed and synthetic spectra (dashed red lines and solid black lines respectively) fitted using the MIDAS code (left figures) and their respective ζ over the Zn line for the fit (right figures).

abundances after changing the input parameters one by one to their upper and lower limits. This is done with the absolute abundances[3].The errors of the stellar parameters are presented in Table 2.1 and the resulting zinc abundances are presented in Table 2.2. The uncertainties were obtained by taking half the difference between the highest and lowest abundance obtained from tweaking each parameter.

Another source of uncertainty is the placement of the continuum level of the observed spectra. When comparing the synthetic and the observed spectra, the two are aligned so that the parts of the spectra that are relatively void of spectral lines coincide. If the continuum is not placed correctly it will result in the wrong line depth and ultimately the wrong abundance.

For the typical spectra fitting, the synthesised spectra that was determined to be the best fit appears to fit about as well as next higher or lower abundance spectra. A reasonable estimation of the error is therefore as large as the zinc abundance step size of 0.06 for the synthetic spectra. The worst fitting spectra that were still included appears to have approximately double this error. Some of the worse fitting spectra were tweaked by hand which resulted of a change in abundance of up to approximately 0.1 dex. Here I assume an upper limit of the abundance uncertainty caused by imperfect fitting to be 0.12 dex, or 2 abundance steps in the fitting procedure. This error should be reduced by a factor of $\sqrt{N}$

[3]The absolute abundance is defined as $\mathrm{A(Zn)} \equiv \log \epsilon(\mathrm{Zn}) = \log \frac{\mathrm{N_{Zn}}}{\mathrm{N_H}} + 12$

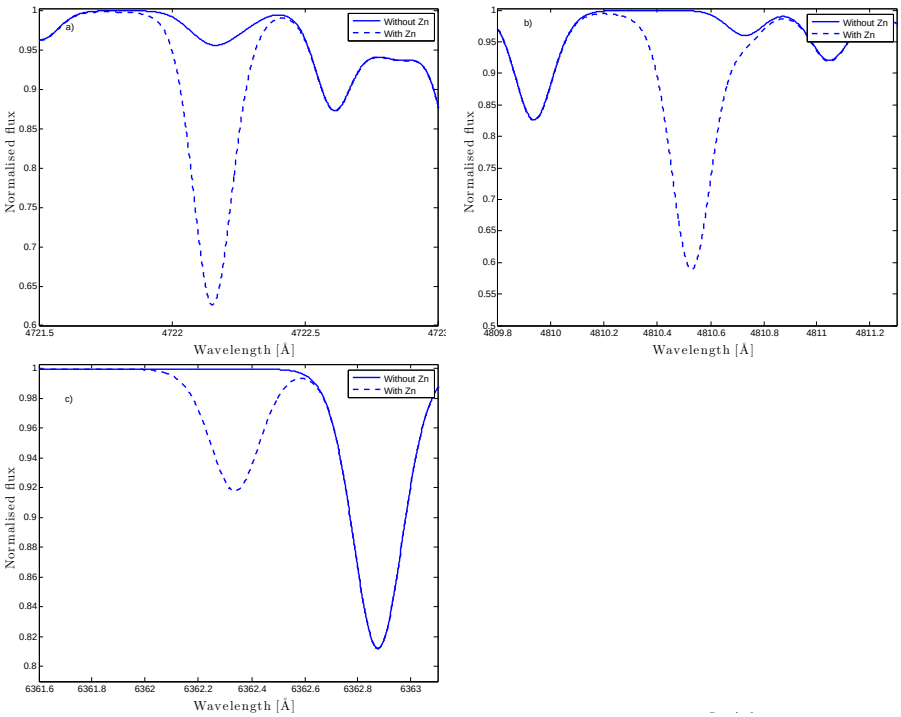

Figure 2.2: Synthetic spectra with and without the zinc spectral lines (dashed and solid lines respectively) and with the parameters of HIP56557 ($T = 5518K, \log(g) = 4.43, [Fe/H] = -0.1, \xi = 0.81km/s$). The zinc lines are generated with the obtained best-fit abundances for each line ($A(Zn)_{4722} = 4.572, A(Zn)_{4811} = 4.733, A(Zn)_{6362} = 4.504$). a): 4722Å line, b): 4811Å line, c): 6362Å line.

where N is the number of spectra that were used to obtain the mean abundance. For most of the spectra this results in a fitting error of $\Delta A(Zn)_{\text{fit}} = \frac{0.12}{\sqrt{3}} \approx 0.07\,\text{dex}$.

All of these errors were then combined according to Eq. 2.1 to give us a total uncertainty (Table 2.2). Errors due to the uncertainty of the stellar parameters are probably smaller than the errors caused by the fitting procedure. Improving the measurements of stellar parameters would probably only result in a tiny reduction of the final uncertainty while an improved fitting procedure could greatly reduce the final uncertainty. The total random error is still significantly smaller than the spread of [Zn/Fe] ratio which suggests an intrinsic variation of [Zn/Fe] in the stars.

$$\Delta A(Zn)_{\text{random}} = \sqrt{\Delta A(Zn)_{T}^2 + \Delta A(Zn)_{\log(g)}^2 + \Delta A(Zn)_{[Fe/H]}^2 + \Delta A(Zn)_{\text{micro}}^2 + \Delta A(Zn)_{\text{fit}})^2} \tag{2.1}$$

For the 6362Å spectral line there is an added uncertainty due to a broad spectral line that was not included in the VALD3 database extract and therefore it was not compensated for by the spectral synthesis. An attempt was made to remove this spectral line for all the observed spectra but a small artefact remained in the spectra. This is likely to affect the

effective line depth of the zinc spectral line and thus also the abundance.

Another problem with the 6362Å line was that it was relatively weak. This means that for stars with a low zinc abundance, the spectral line was barely visible over the noise. This added extra uncertainty to stars with low zinc abundance although the results from the other two lines should somewhat make up for it.

Table 2.1: Stellar parameters and their errors of selected stars.

HIP	T_{eff}	ΔT_{eff}	$log(g)$	$\Delta log(g)$	[Fe/H]	Δ[Fe/H]	ξ	$\Delta\xi$
59696	5055	48	3.41	0.09	-0.74	0.05	1.09	0.07
75487	6455	52	4.14	0.09	-0.66	0.03	1.84	0.13
85963	6535	62	4.13	0.10	-0.61	0.04	2.17	0.16
87679	5357	123	4.34	0.14	0.11	0.15	0.67	0.15
103609	4993	45	3.74	0.09	-0.31	0.04	0.80	0.07
114962	5935	68	4.32	0.10	-1.50	0.06	1.63	0.37

Table 2.2: Random errors in the Zn abundances due to the uncertainties of stellar parameters and due to the imperfect fitting as well as the combined total random error.

HIP	$\Delta A(Zn)_{T}$	$\Delta A(Zn)_{log(g)}$	$\Delta A(Zn)_{[Fe/H]}$	$\Delta A(Zn)_{\xi}$	$\Delta A(Zn)_{fit}$	$\Delta A(Zn)_{random}$
59696	0.003	0.027	0.008	0.021	0.07	0.08
75487	0.024	0.008	0.001	0.013	0.07	0.07
85963	0.025	0.006	0.005	0.010	0.07	0.07
87679	0.033	0.013	0.028	0.049	0.07	0.1
103609	0.016	0.021	0.013	0.023	0.07	0.07
114962	0.017	0.022	0.003	0.009	0.07	0.07

Chapter 3

Results and discussion

3.1 Zinc abundances

The obtained [Zn/Fe] ratios are plotted against their stars metallicity in figure 3.5b. The zinc to iron ratio that was obtained through our simulations appears to follow a mostly flat trend but with slightly lower spread in the [Zn/Fe] ratio for lower metallicity stars. Thick disk stars generally have a lower metallicity and they also have a somewhat higher [Zn/Fe] ratio compared to the thin disk stars, even compared to the thin disk stars with similar [Fe/H] ratio. There is a small increase in [Zn/Fe] ratio in the intermediate metallicity stars although it appears to be at a higher [Fe/H] than expected and appears almost completely absent for the thin disk stars. The drop in [Zn/Fe] ratio after this 'bump' is also not very severe. These trends are not very clear since the spread in [Zn/Fe] ratios is rather large and the sample size is very small for stars with [Fe/H] < -1.

3.2 Comparison between results

The purpose of this project was to improve the results obtained by Bensby et al. (2014) so it makes sense to compare their abundances with ours. The abundance results from the individual lines were also compared to try and identify systematic errors unique to a particular line. The final results gathered in this work are all normalised with respect to the solar abundance obtained through the same synthesis method. This should eliminate some of the systematic errors of the method. It is clear that there is still some systematic difference between the results obtained from the different spectral lines (see fig. 3.1). There also appears to be some systematic difference in the spread and the difference in abundance from the different lines depending on which observation the studied spectra comes from. This suggests that there could be some problem with some spectra, such as a non-linear response to the flux. The abundances obtained from the august 2005 observations appear to have a noticeably better agreement for all three spectral lines.

When plotting the results from the three spectral lines individually, a large spread in [Zn/Fe] is observed for the 4722Å and 4811Å lines while the 6362Å line had a relatively

small spread in [Zn/Fe] (see fig. 3.6). The results from the 6362Å line also show an increase in [Zn/Fe] for lower metallicity stars, although the results from this line at low metallicities are uncertain due to the weakness of the spectral line.

The abundances obtained from the 4722Å line are consistently lower than for the other two lines and the abundances from Bensby et al. (2014) (see figures 3.1a, 3.1b and 3.3a). The abundances obtained from the 4811Å line are lower for the low abundance spectra and higher for the high abundance spectra, compared to the results from the other spectral lines and from Bensby et al. (2014) (see figures 3.1a, 3.1c and 3.3b). The abundances obtained from the 6362Å spectral line have significantly smaller spread than the other two lines (see fig. 3.2). The 6362Å results are in good agreement with the abundances by Bensby et al. (2014) (figure 3.1c). The averaged abundances for the three spectral lines does not differ significantly from the abundances obtained by Bensby et al. (2014) (3.3d). The spread in [Zn/Fe] ratios for a given metallicity appears to be similar in magnitude as well, i.e. there doesn't appear to be much improvement in the precision under the assumption that the observed spread is caused by measurement and fitting errors. The standard deviation of the [Zn/Fe] ratio is the same for both studies at well at $\sigma(\mathrm{Zn/Fe}) = 0.12\,\mathrm{dex}$. The obtained zinc abundances are generally lower than the values obtained by Bensby et al. (2014). This was expected due to the blending lines for the 4722Å and 4811Å zinc lines. However, this overestimation was also expected to be lower for solar metallicity stars since the solar analysis should have accounted for the overestimation in these cases. Figure 3.5c shows approximately the same overestimation for stars of all metallicities. It would be interesting to see if this difference between the results would be reduced if the methodology here was repeated without the inclusion of the blending lines. Another possibility is that this difference is caused by the solar abundances obtained for the 4722Å and 4811Å lines. The analysis of the Vesta and Ceres exposures differed by approximately 0.4 dex in both of these cases. This suggests a large uncertainty in the solar abundance for these lines and by extension this would mean a systematic error for all the values obtained from the 4722Å and 4811Å lines since the final abundance is normalised with respect to the solar abundance.

3.3 Precision of results

There is no apparent reduction in the spread of zinc abundances compared to Bensby et al. (2014). If the spread in zinc abundances truly is due to uncertainty caused by the methodology, then there doesn't seem to be any improvement of the line synthesis method over the equivalent width based measurements. The error analysis conducted in this work suggests that the uncertainty of these abundances is significantly smaller than their observed spread. It is expected that some small improvement in the abundances could be achieved by manually going through the alignment process for each line in every spectra. This was done for a few spectra and the difference in A(Zn) abundance after tweaking the fit could be as large as 0.1 dex for cases where the automatic fit was particularly bad. This is because some lines appear to be slightly misaligned by the MIDAS script while

others appear to be placed correctly. However, some of the alignment process could not be corrected by hand; the placement of the continuum is difficult for some spectra, particularly for low s/n spectra. The presence of a broad spectral line caused by Ca auto ionisation (Mitchell & Mohler 1965) that was blended with the 6362Å line and absent from our line lists is another source of error. Although an attempt was made to eliminate this line by fitting a spline function to continuum points, there was obviously an artefact remaining on the spectra despite this. It should be possible to reduce the presence of this artefact either by improving the method used to eliminate the spectral line or by identifying the cause and obtaining the correct line data to properly synthesise it, although this is beyond the scope of this thesis. The error from this spectral line is probably of a similar nature as the error from an equivalent width based method caused by blended spectral lines that are not accounted for.

As mention in sect. 3.2, the solar zinc abundance obtained from the 4722Å and the 4811Å lines, the different solar spectra yielded significantly different abundances. This discrepancy is unexpected because all the included synthetic solar spectra appeared to fit well with the observed solar spectra (see fig. 3.4). The reason for this discrepancy does not appear to be due to the fitting process. There does seem to be a difference in the depth in the Vesta and Ceres spectra for some of the spectral lines even though the abundances and stellar parameters should be the same since its the same star. This discrepancy is not seen for the 6362Å line. The spread in the abundances obtained from the 4722Å and the 4811Å lines is also significantly greater than for the abundances obtained from the 6362Å line. When discussing these problems with my supervisor, he expressed concern over the quality of the blue spectra where 4722Å and 4811Å lines are situated. There is a possibility of a non-linear response to the flux in the blue CCD. If this is the case then it would distort the spectra and add errors to any abundance analysis conducted using these spectra. This added error could mean that the high spread in [Zn/Fe] is not intrinsic but in fact caused by measurement errors. Moehler et al. (2014) expresses the need for new standard star catalogues for the flux calibration of high resolution spectra due to the coarse sampling of previous standard star catalogues. Perhaps the perceived problem is caused by such a calibration error. In order to assess the quality of the calibration of the spectrograph, the spectrograph response should be compared to high resolution reference spectra (e.g. Moehler et al. 2014).

3.4 Thick or thin disk

Whether a given star is part of the thick or the thin disk, to a reasonable approximation, was determined in Bensby et al. (2014) by studying the kinematic properties of the star. Any star with a thick disk-to-thin disk probability ratio (TD/D)[1] greater than 2 is considered

[1]The thick disk (TD) and thin disk (D) probabilities were determined by Bensby et al. (2014) by comparing the stellar velocities with characteristic velocities for stars in the thick and thin disks respectively (larger TD if the velocity of a star is similar to the characteristic thick disk velocity). TD/D is the ratio between the probabilities (see appendix A in Bensby et al. (2014) for a detailed explanation).

a thick disk star and any star with a TD/D ratio lesser than 0.5 is considered a thin disk star. Stars with a TD/D ratio between 0.5 and 2 are considered in between the thick and the thin disks. No major difference in the [Zn/Fe] ratio is observed for the different disks but there appears to be a slightly lower [Zn/Fe] ratio for intermediate metallicity thin disk stars with [Fe/H] < -0.2.

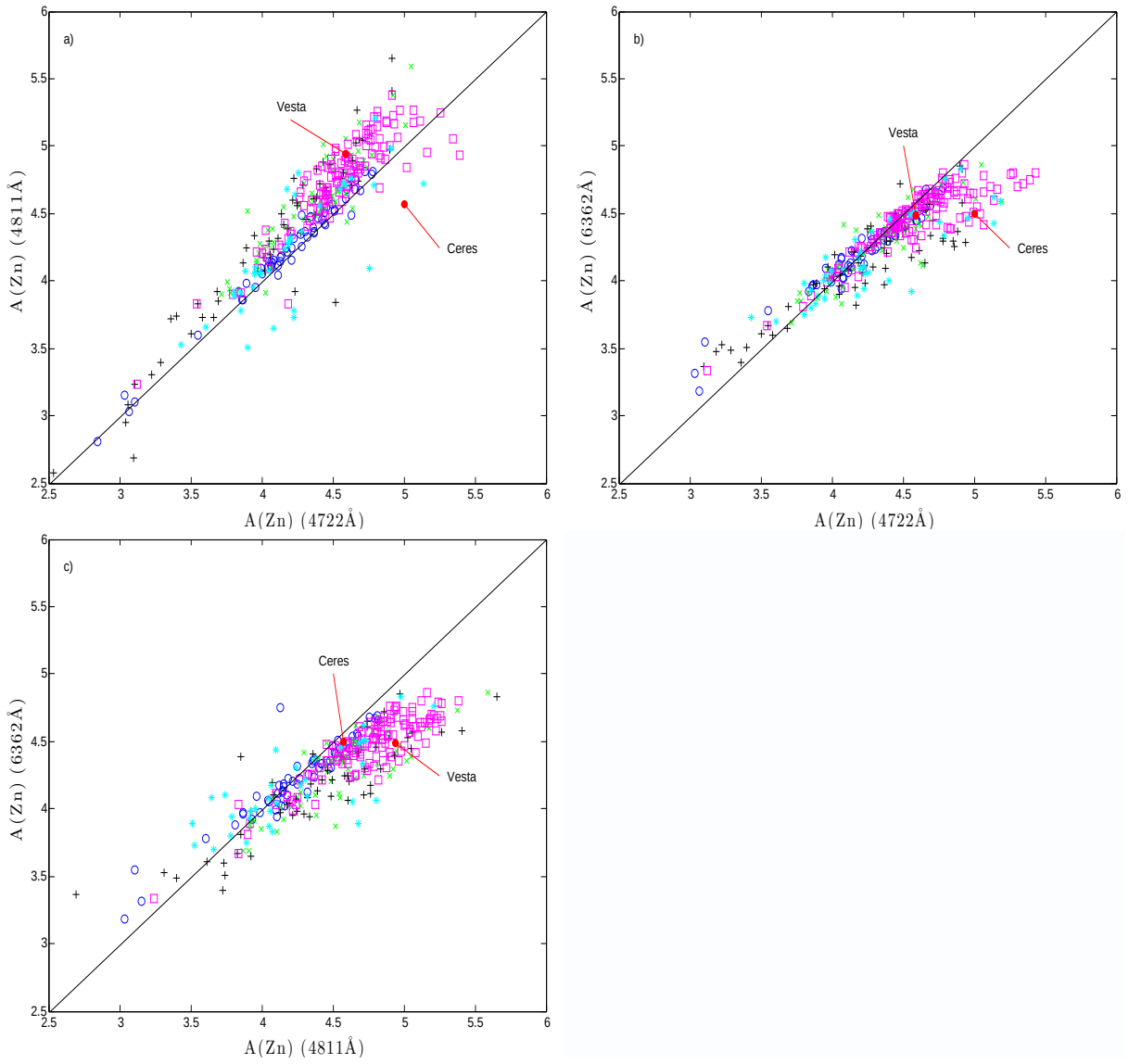

Figure 3.1: Comparison between the results obtained from: a) the 4722Å and the 4811Å lines, b) the 4722Å and the 6362Å lines, and c) the 4811Å and the 6362Å lines. Blue circles, green crosses, black plusses, magenta squares and cyan asterixes show observations from august 2005, january 2006, april 2006, august 2006 and april 2007 respectively. Filled red dots show values obtained for the Sun. The Vesta observations are from january 2006 and the Ceres observations are from august 2006.

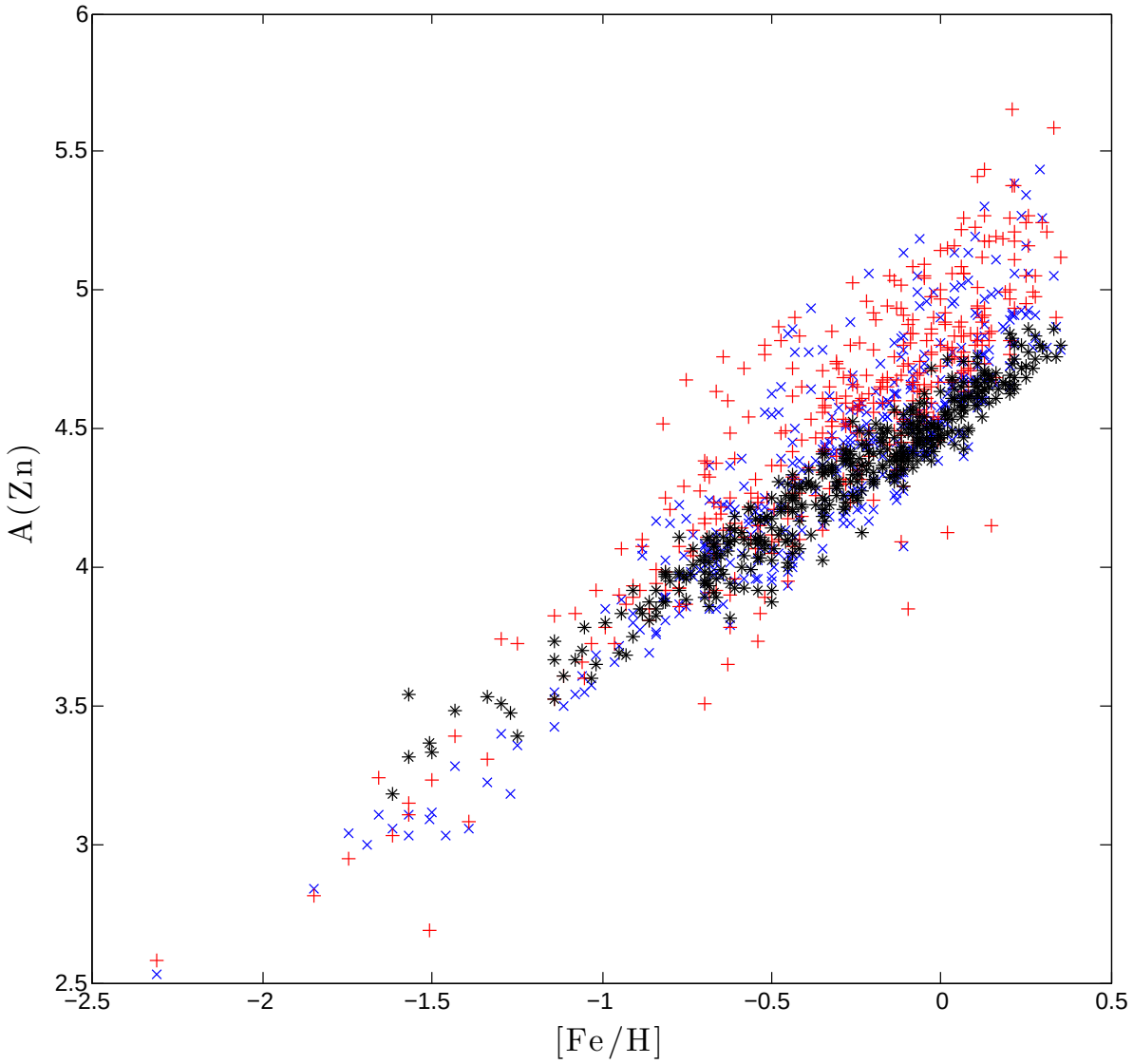

Figure 3.2: Absolute zinc abundances obtained for all three lines. Blue crosses, red plusses and black asterixes show abundances obtained from the 4722Å line, the 4811Å line, and the 6362Å lines, respectively

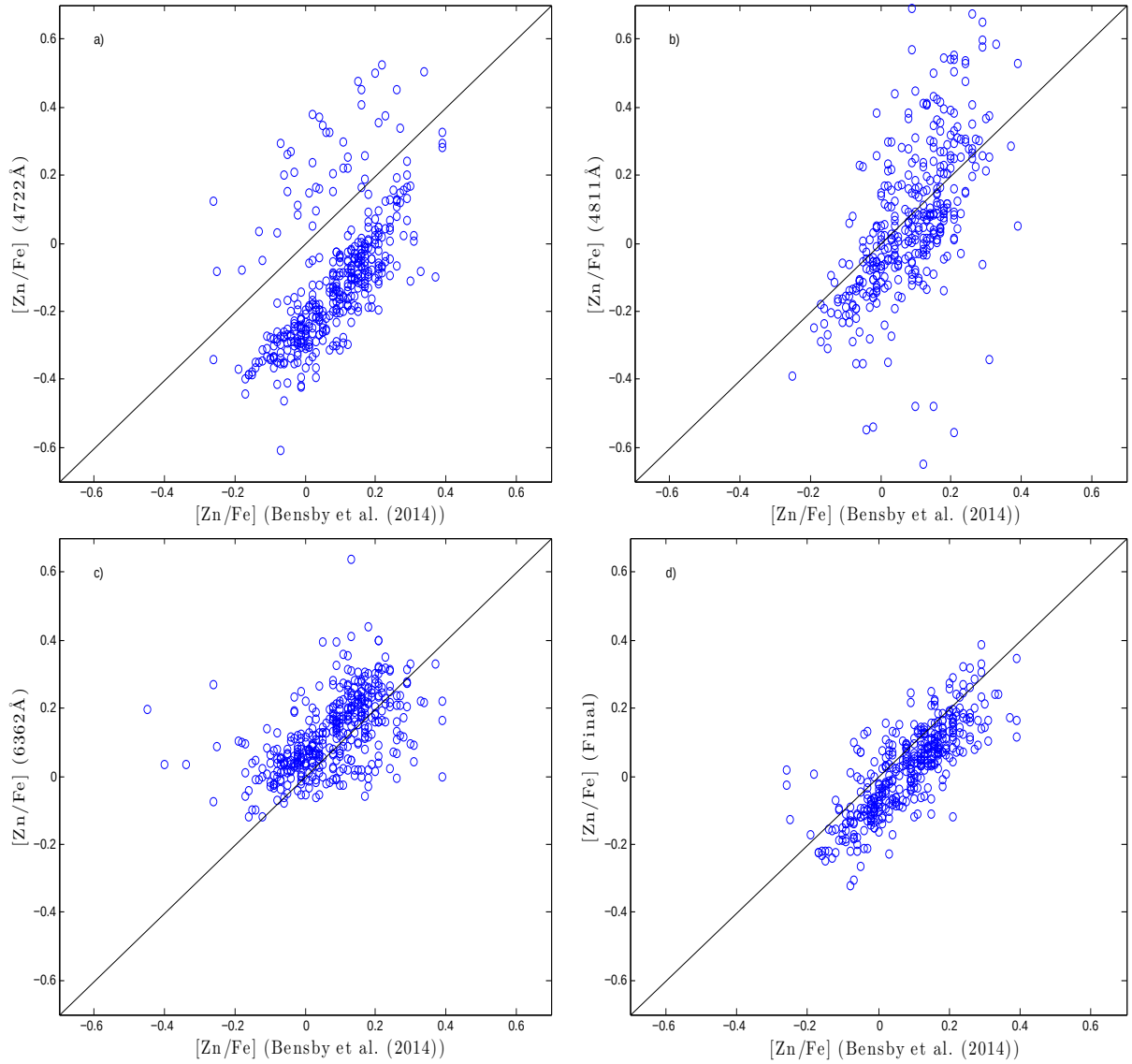

Figure 3.3: Comparison between the results obtained by Bensby et al. (2014) and: a) the 4722Å line, b) the 4811Å line, c) the 6362Å line, and d) the average for all lines

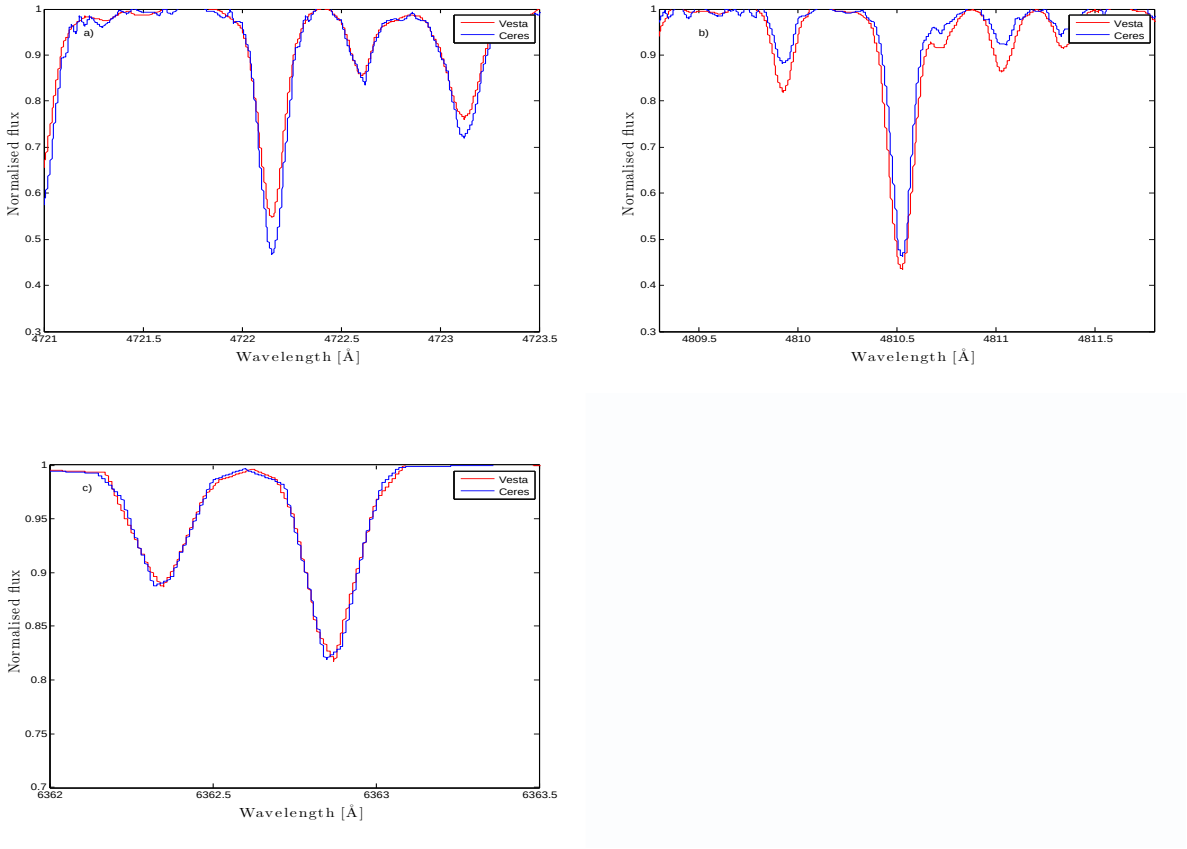

Figure 3.4: Observed spectra of the Sun. Red and blue lines show exposures of Vesta and Ceres respectively. a): 4722Å line, b) 4811Å line, and c) 6362Å line. The obtained abundances differ significantly for the 4722Å and 4811Å lines and there is an obvious difference in line depth for the different exposures. This problem is not present for the 6362Å line that is part of the spectra from the red CCD plates.

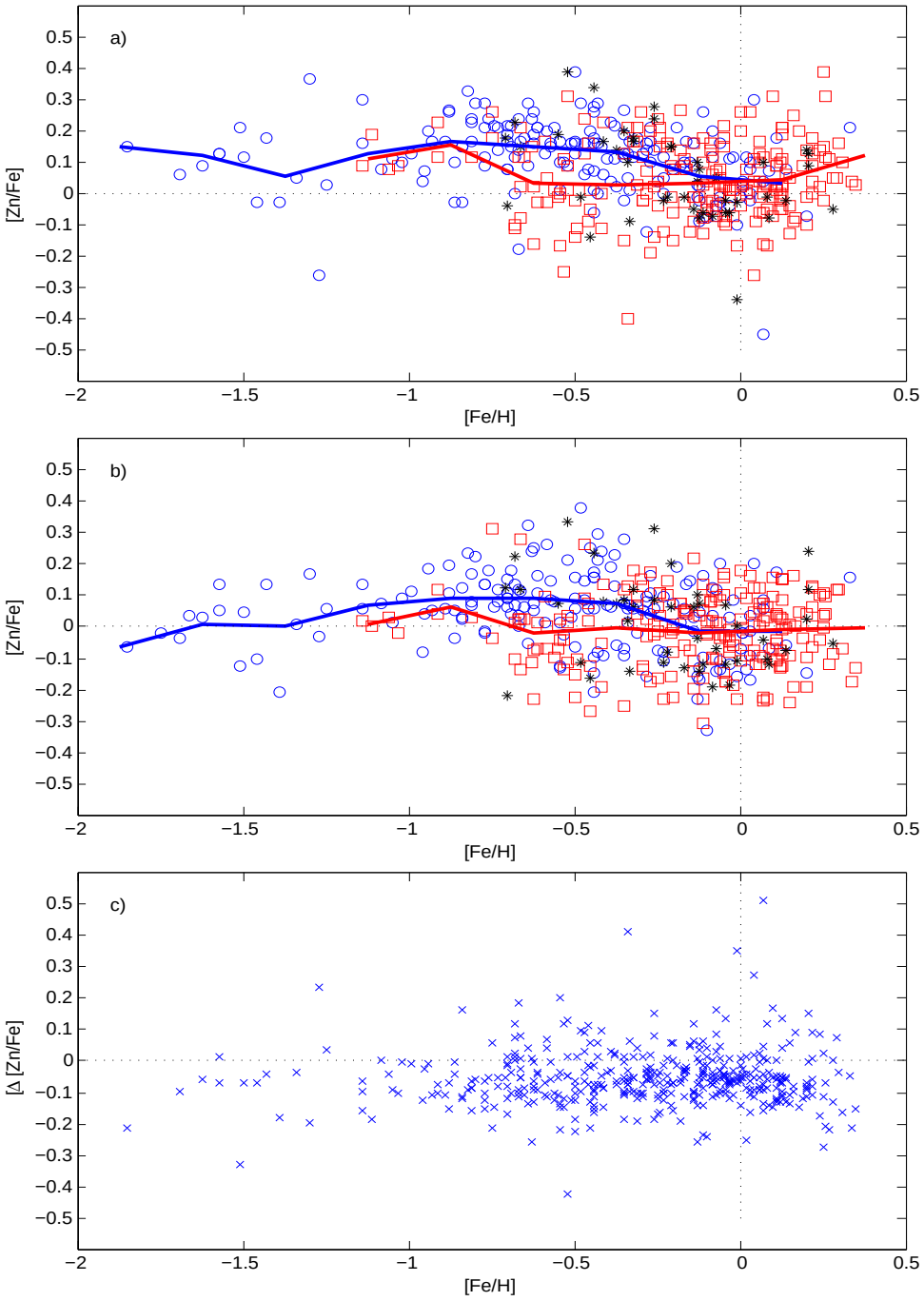

Figure 3.5: Zn/Fe ratios from a) Bensby et al. (2014) and b) this work. Only stars present in both studies are shown. Thick disk stars are shown with blue circles, thin disk stars are shown with red squares and in-between stars are shown with black asterisk. The blue and red lines show average values for the thick and thin disks respectively. The difference in Zn/Fe ratios between the studies are shown in c).

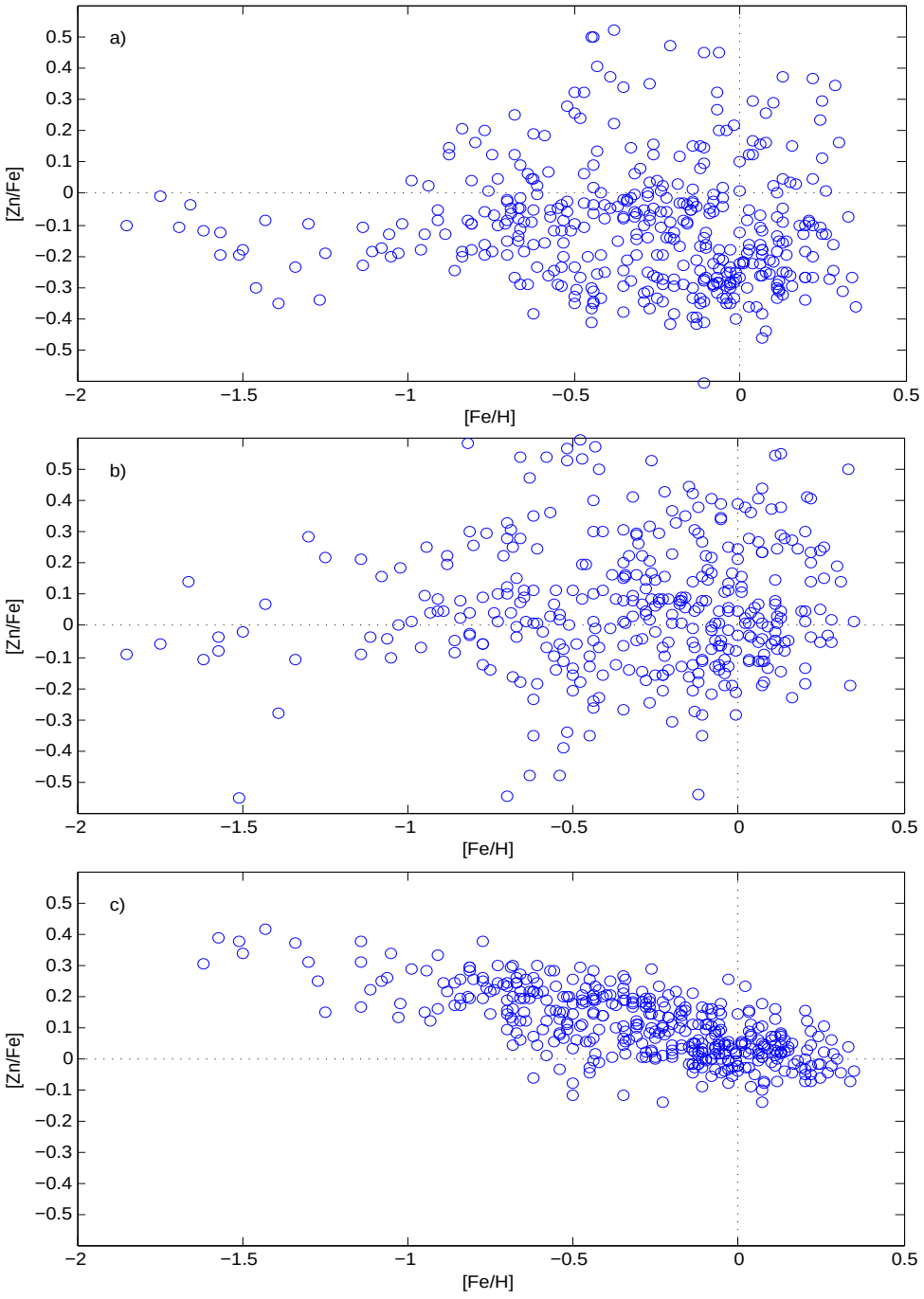

Figure 3.6: Zn/Fe ratios obtained from a) the 4722Å line, b) the 4811Å line and c) the 6362Å line.

Chapter 4

Conclusions

Due to the absence of any improvement over the results from Bensby et al. (2014), not much new insight can be gained on zinc's suitability as a proxy for iron or the cosmic origin of zinc. There does seem to be a weak trend towards lower [Zn/Fe] ratio at both higher and lower metallicities and consequently a relatively high [Zn/Fe] ratio for intermediate metallicity stars. The decrease in [Zn/Fe] at higher metallicities is less than expected if we assume that high metallicity stars get half of their iron but relatively negligible amounts of zinc from SNIa as suggested by Nomoto et al. (1997). The drop in [Zn/Fe] ratio also occurs at a higher metallicity than expected. Still, these results suggest that SNIa are relatively minor sources of zinc enrichment in the universe.

Although the sample size at lower metallicities is too low for any definite conclusions, there appears to be an increase in [Zn/Fe] with increasing [Fe/H] at lower metallicities. This is consistent with an increasing [Zn/Fe] yield from SNII with increasing metallicity of the progenitors.

The suitability of zinc as a proxy for iron depends on the desired precision of the iron measurements. Although the average [Zn/Fe] ratio is near 0 for all metallicities, the large spread would make such measurements uncertain. The standard deviation of $\sigma(\mathrm{Zn/Fe}) = 0.12\,\mathrm{dex}$ gives us an estimate of the expected error when obtaining the [Fe/H] ratio from the [Zn/H] ratio. Although some of this error could be due to the methodology and could be improved, the error analysis performed here suggests that a large component of the spread is intrinsic to the stars. It is also important to note that the [Zn/Fe] ratio may deviate slightly for different metallicities. Unless this deviation is considered, iron abundances are likely to be slightly overestimated for intermediate metallicity stars.

The sample used in this work contains mostly high metallicity stars and not much can be learned about the [Zn/Fe] trends at the lower metallicites from the results presented here. Further studies on low metallicity samples warranted.

Acknowledgements. I want to thank my supervisor Thomas Bensby for his guidance during the making of this thesis. I want to thank my mother and father for convincing me to continue with my education.

Bibliography

Bensby, T., Feltzing, S., & Oey, M. S. 2014, A&A, 562, A71

Bernstein, R., Shectman, S. A., Gunnels, S. M., Mochnacki, S., & Athey, A. E. 2003, in Society of Photo-Optical Instrumentation Engineers (SPIE) Conference Series, Vol. 4841, Instrument Design and Performance for Optical/Infrared Ground-based Telescopes, ed. M. Iye & A. F. M. Moorwood, 1694–1704

Ishigaki, M. N., Aoki, W., & Chiba, M. 2013, ApJ, 771, 67

Kobayashi, C. & Nomoto, K. 2009, ApJ, 707, 1466

Kobayashi, C., Umeda, H., Nomoto, K., Tominaga, N., & Ohkubo, T. 2006, ApJ, 653, 1145

Kupka, F., Piskunov, N., Ryabchikova, T. A., Stempels, H. C., & Weiss, W. W. 1999, aaps, 138, 119

Kupka, F. G., Ryabchikova, T. A., Piskunov, N. E., Stempels, H. C., & Weiss, W. W. 2000, Baltic Astronomy, 9, 590

Mitchell, Jr., W. E. & Mohler, O. C. 1965, ApJ, 141, 1126

Moehler, S., Modigliani, A., Freudling, W., et al. 2014, A&A, 568, A9

Nomoto, K., Iwamoto, K., Nakasato, N., et al. 1997, Nuclear Physics A, 621, 467

Nomoto, K., Kobayashi, C., & Tominaga, N. 2013, ARA&A, 51, 457

Piskunov, N. E., Kupka, F., Ryabchikova, T. A., Weiss, W. W., & Jeffery, C. S. 1995, aaps, 112, 525

Podsiadlowski, P., Mazzali, P. A., Nomoto, K., Lazzati, D., & Cappellaro, E. 2004, ApJ, 607, L17

Prieto, J. L., Stanek, K. Z., & Beacom, J. F. 2008, ApJ, 673, 999

Ryabchikova, T. A., Piskunov, N. E., Kupka, F., & Weiss, W. W. 1997, Baltic Astronomy, 6, 244

Tominaga, N., Umeda, H., & Nomoto, K. 2007, ApJ, 660, 516

Tsujimoto, T., Nomoto, K., Yoshii, Y., et al. 1995, MNRAS, 277, 945

Valenti, J. A. & Fischer, D. A. 2005, ApJS, 159, 141

Valenti, J. A. & Piskunov, N. 1996, aaps, 118, 595

Appendix A

Linelists

The linelist used to synthesise the 4722Å spectra was obtained from VALD3 the 2015/02/10 using the parameters in Table A.1 for lines between 4717Å and 4727Å. The Si I line at 4721.57Å was removed due to it not being present in any of the observed spectra.

The linelist used to synthesise the 4811Å spectra was obtained from VALD3 the 2015/02/09 using the parameters in Table A.1 for lines between 4806Å and 4816Å. The $\log gf$ of the Cr I line at 4810.73Å was changed from -0.644 to -1.5 to better coincide with the observed lines.

The linelist used to synthesise the 6362Å spectra was obtained from VALD3 the 2015/02/11 using the parameters in Table A.1 for lines between 6357Å and 6367Å.

Table A.1: Parameters used to extract the VALD3 linelists.

Parameter	Value
Detection threshold	0.005
Microturbulence	1.00
Effective temperature	5780
$\log g$	4.4

Table A.2: Line data used for the synthesis of the 4722Å line.

Spec Ion	$\lambda(\AA)$	log gf	Element	$\lambda(\AA)$	log gf	Element	$\lambda(\AA)$	log gf
Nd II	4717.0850	-1.600	Fe I	4720.5598	-3.192	Ni I	4723.3466	-2.836
C2 I	4717.1689	-0.353	Fe I	4720.9624	-1.999	C2 I	4723.3590	-0.403
CH I	4717.1920	-2.798	Fe I	4721.0005	-2.801	C2 I	4723.3601	-0.414
C2 I	4717.1993	-0.363	Ca II	4721.0220	-2.197	C2 I	4723.4565	-0.424
Fe I	4717.2331	-4.822	C2 I	4721.0427	-0.393	Ni I	4723.8823	-2.529
C2 I	4717.2898	-0.372	C2 I	4721.0662	-0.382	C2 I	4724.3319	-0.414
Cr I	4717.6840	-1.750	Cr I	4721.1258	-1.766	C2 I	4724.3338	-0.424
V I	4717.6935	-0.242	C2 I	4721.1982	-0.403	Nd II	4724.3600	-0.430
Sm II	4717.7300	-0.910	Co I	4721.4003	-0.286	Cr I	4724.4120	-0.647
Ce II	4717.8810	-1.140	V I	4721.5103	-0.264	La II	4724.4220	-1.820
Fe I	4718.1354	-3.034	C2 I	4722.0950	-0.393	C2 I	4724.4242	-0.435
Fe I	4718.3042	-4.865	C2 I	4722.1192	-0.403	Ca I	4724.5297	-0.793
Sm II	4718.3400	-0.820	Zn I	4722.1530	-0.338	Ti I	4724.6617	-1.530
Cr I	4718.4190	0.240	Fe I	4722.1720	-3.164	Ce II	4725.0690	-1.440
Co I	4718.4688	0.138	Cr I	4722.1871	-1.135	Fe I	4725.3223	-3.232
Ce II	4718.4786	-1.620	C2 I	4722.1932	-0.413	C2 I	4725.4483	-0.424
C2 I	4718.5982	-0.363	Sr I	4722.2740	-0.220	C2 I	4725.4672	-0.436
C2 I	4718.5991	-0.373	Ce II	4722.2929	-1.470	C2 I	4725.5943	-0.447
C2 I	4718.6925	-0.382	Ti I	4722.6059	-1.470	Cr I	4725.6630	-1.416
Fe I	4719.1103	-3.419	Cr I	4722.6500	-1.940	Fe I	4725.8115	-3.383
Zr I	4719.1200	0.050	Cr I	4722.7600	-1.272	Ce II	4725.0974	-0.670
Fe I	4719.2186	-2.339	V I	4722.8709	-0.130	Cr I	4725.9230	-2.231
Ti II	4719.5109	-3.320	Ni I	4723.0012	-1.742	Fe I	4725.9381	-2.965
Ni I	4719.6675	-1.377	Cr I	4723.0146	-0.937	Sm II	4726.0300	-1.250
C2 I	4719.6963	-0.373	Cr I	4723.0980	-0.660	Fe I	4726.1370	-3.250
C2 I	4719.7639	-0.382	Ni I	4723.1302	-1.655	C2 I	4726.3121	-0.447
C2 I	4719.8380	-0.392	Ni I	4723.1422	-3.049	C2 I	4726.3478	-0.435
Sm II	4719.8400	-1.240	Cr I	4723.1520	-0.661	C2 I	4726.4962	-0.458
La II	4719.9190	-0.450	Ti I	4723.1631	-1.480	CH I	4726.7030	-2.834
Sm II	4720.1300	-1.620	Ce II	4723.3210	-1.380	CH I	4726.7550	-2.814
Fe II	4720.1386	-4.822	Cr II	4723.3395	-2.784	Si I	4726.8288	-2.743
Cr I	4720.5184	-1.418	Fe I	4723.3431	-2.850			

Table A.3: Line data used for the synthesis of the 4811Å line.

Spec Ion	$\lambda(\AA)$	log gf	Element	$\lambda(\AA)$	log gf	Element	$\lambda(\AA)$	log gf
Ti II	4805.0850	-0.960	Cr I	4807.8111	-1.933	Ni I	4811.9829	-1.480
Fe I	4805.0981	-2.568	Fe I	4808.1478	-2.790	CH I	4811.9900	-2.546
CH I	4805.1320	-2.973	Co I	4808.2260	-0.976	CH I	4811.9930	-2.562
Cr I	4805.2640	-0.400	Ti I	4808.5261	-0.130	Ti I	4812.2324	-0.580
Fe I	4805.3169	-1.182	Fe I	4808.5349	-4.652	Cr I	4812.2333	-1.034
Ti I	4805.4144	0.070	Ni I	4808.5479	-1.751	CH I	4812.2640	-2.464
Si I	4805.4386	-2.700	Fe I	4808.6795	-1.296	CH I	4812.3290	-2.448
Fe I	4805.5245	-2.717	Ni I	4808.8740	-1.410	Cr II	4812.3370	-1.960
Zr I	4805.8700	-0.420	La II	4809.0000	-1.400	Ni I	4812.8922	-1.640
Cr I	4805.9600	-0.853	Fe I	4809.1371	-2.228	Ti I	4812.8934	-3.280
Ce II	4806.2028	-0.920	CH I	4809.2370	-2.435	Fe I	4813.1128	-2.890
Cr I	4806.2500	-1.870	Fe I	4809.2518	-3.378	Co I	4813.4555	-1.520
Ti II	4806.3210	-3.380	Cr I	4809.2850	-1.499	Co I	4813.4764	0.120
CH I	4806.7420	-2.870	CH I	4809.3080	-2.448	Fe I	4813.7202	-2.430
Ti I	4806.7584	-2.990	Zr I	4809.4700	0.160	V II	4813.9495	-1.518
Mn II	4806.8226	-1.848	Cr I	4809.9326	-1.816	Co I	4813.9717	-0.905
Ni I	4806.9872	-0.640	Fe I	4809.9326	-1.891	CH I	4814.2460	-3.047
CH I	4807.0080	-2.448	Fe I	4809.9384	-2.720	Cr I	4814.2660	-1.220
CH I	4807.0500	-2.435	Cr I	4810.0376	-1.144	CH I	4814.3000	-2.448
CH I	4807.0550	-2.870	Zn I	4810.5280	-0.137	CH I	4814.3430	-2.464
Mn I	4807.1573	-1.170	Cr I	4810.7300	-1.500	Fe I	4814.3702	-2.602
Cr I	4807.2022	-1.089	Fe II	4810.7443	-3.287	Cr I	4814.5423	-1.282
Fe I	4807.2308	-2.331	Ti I	4811.0311	-2.299	Fe II	4814.5441	-7.735
Fe I	4807.2847	-3.997	Fe I	4811.0332	-3.533	Ni I	4814.5910	-1.620
CH I	4807.4040	-2.532	Ti I	4811.0679	-0.391	CH I	4814.6180	-3.004
V I	4807.5207	0.380	Nd II	4811.3420	-1.140	CH I	4814.7440	-2.546
CH I	4807.5590	-2.546	Ti I	4811.5357	-1.421	CH I	4814.8740	-3.047
Fe I	4807.7082	-2.200	Sr I	4811.8770	0.190	CH I	4814.8760	-2.562

Table A.4: Line data used for the synthesis of the 6362Å line.

Spec Ion	$\lambda(\AA)$	log gf	Element	$\lambda(\AA)$	log gf	Element	$\lambda(\AA)$	log gf
Si I	6352.9535	-2.389	V I	6358.8164	-0.762	Fe I	6364.6946	-1.486
Si I	6353.3597	-0.594	Ti I	6359.1733	-2.230	Nd II	6365.5396	-1.200
Si I	6353.5188	-0.728	Ti I	6359.8884	-4.070	Co I	6366.2899	-0.808
Ca I	6353.5479	-0.523	Ca I	6360.2983	-0.626	Ti I	6366.3468	-1.640
Si I	6354.9025	-2.352	Fe I	6360.7358	-1.909	Ni I	6366.4805	-0.874
Fe I	6355.0281	-2.350	Ni I	6360.8107	-1.027	Fe I	6366.7104	-2.509
Si I	6355.3941	-2.979	V I	6361.2522	-0.872	Fe I	6368.6248	-1.829
V I	6355.5824	-1.148	Ti I	6361.3365	-2.220	Fe I	6369.2167	-2.344
Mn I	6356.0657	-1.424	Zn I	6362.3380	0.150	Fe II	6369.4590	-4.160
V I	6357.2920	-0.910	Cr I	6362.8620	-3.119	Cr I	6369.6603	-1.833
La II	6358.1050	-1.940	Fe I	6362.8758	-1.970	Ni I	6370.3458	-1.940
Fe I	6358.6324	-1.657	Fe I	6362.8900	-1.970	Si I	6370.5744	-0.947
Fe I	6358.6531	-3.448	O I	6363.7760	-10.258	Ce II	6371.1090	-0.620
Ti I	6358.6871	-2.890	Fe I	6364.3640	-1.430	Si II	6371.3714	-0.040
Fe I	6358.6967	-4.468	Ni I	6364.5715	-3.970	Ti I	6371.4957	-1.940

Appendix B

Excluded spectra

Results from the analysis of one or more lines for some stars were excluded because the observed and synthetic spectra could not be made to coincide to an acceptable level. Table B.1 lists these instances of exclusion along with a number depending on the reason for the exclusion. 0 = not excluded for this line, 1 = problems fitting spectra (mostly due to issues with the MIDAS code that was used to fit the spectra), 2 = wrong broadness of spectral line, probably due to overexposure (the 4811Å line was particularly susceptible to this, probably due to the sensor being extra sensitive around this wavelength), 3 = very low s/n around the spectral line.

Table B.1: Excluded spectra along with the reason for their exclusion.

HIP	4722Å	4811Å	6362Å	HIP	4722Å	4811Å	6362Å
1955	1	1	0	62534	0	2	0
6177	0	1	0	68464	1	1	3
6856	0	1	0	70182	0	2	0
7091	1	1	0	71844	0	1	0
8498	0	1	0	72797	2,3	2,3	3
13902	1	1	0	74234	0	0	1
14339	0	1	0	74235	0	3	1
18802	1	0	0	76976	1	1	3
19233	1	1	0	77637	0	0	1
19773	0	1	0	79138	0	0	1
20638	1	1	0	80587	1	1	0
22278	1	1	0	81269	0	2	0
24037	0	1	0	81580	0	1	0
24682	1	1	0	81952	0	1	0
25528	1	1	0	86694	0	0	1
34254	0	2	0	87154	0	1	0
34285	0	0	1	87539	1	0	0
35718	0	2	0	89583	1	1	0
36269	0	0	1	89881	1	0	0
37233	0	1	0	90365	0	1	0
37419	0	1	0	91471	0	1	0
42889	0	0	1	93186	0	0	3
45514	0	2	0	93377	0	1	0
46888	0	2	0	96881	0	0	1
47588	0	2	0	98020	0	1	3
50713	0	2	0	99174	0	1	0
53719	0	0	1	101346	1	1	0
54469	0	2	0	101399	0	1	0
54779	0	2	0	103881	1	1	0
57360	0	1	0	106701	0	1	0
58153	0	2	0	109110	0	1	0
58843	0	1	0	110843	0	1	0
59532	2	2	0	111274	1	1	0
60462	0	2	0	112201	1	1	0
60574	0	2	0	113113	0	1	0
60632	0	0	1,3	114702	1	1	0
60729	0	2	0	115917	1	1	0